Aggregation of a Zn(II) Complex of a Long-Chain Triester of *meso*-Tetrakis[*p*-carboxy]phenyl Porphyrin in Hydrocarbons: Structure of Tetrameric Rodlike Assemblies

Pierre Terech,*,† Christine Scherer,† Bruno Demé,‡ and René Ramasseul§

UMR 5819 CEA-CNRS-Université J. Fourier, SI3M, Laboratoire Physico-Chimie Moleculaire, 38054 Grenoble Cédex 9, France, Institut Laue Langevin, 6 rue Jules Horowitz, 38042 Grenoble Cédex 9, France, and UMR 5046 CEA-CNRS-Université J. Fourier, SCIB, Laboratoire de Chimie Inorganique et Biologique, 17, rue des Martyrs, 38054 Grenoble Cédex 9, France

Received February 26, 2003. In Final Form: October 9, 2003

It is shown that gelatinous solutions in cyclohexane of a Zn complex of a long-chain triester of *meso*-tetrakis[*p*-carboxy]phenyl porphyrin (ZnP3) are made up of rodlike assemblies. The presence of both Zn atom and carboxylic function, reinforcing the usual $\pi-\pi$ interactions, is determinant for the aggregation. The carboxylic groups in ZnP3 tetramers are associated in the central core of ca. 60 Å diameter rods. J-type lateral aggregation is characterized by a typical Soret exciton absorption. Small-angle neutron scattering profiles are analyzed to detail the network composition as a function of concentration of ZnP3 or of an end-capping molecule such as pyridine. A model of supramolecular organization in the rods is proposed with four ZnP3 molecules laterally associated per section and with a slipped arrangement of consecutive layers in tilted columnar rods.

1. Introduction

Particles in the nanoscale are receiving a great deal of attention due to the potential applications that take advantage of their particular morphology. Such structures might be used for sensor and catalysis technologies while the synthesis of their polymeric or inorganic replicas may open advanced possibilities in the fields of electronics, optoelectronics, or time-controlled chemical release. The self-assembled rodlike morphology can be obtained with a wide variety of small molecules in aqueous or organic media.[1,2]

Among these examples, porphyrins form a highly interesting class. Porphyrins are known to be essential molecules for the harvesting of light energy by plants.[3−5] Supramolecular self-assemblies of porphyrins are also promising systems for oxygen transport, enhanced catalysis, information storage, or engineering of photoactive nanostructures. Strong attractive interactions between porphyrin molecules are responsible for their spontaneous aggregation in aqueous solutions.[6,7] Pseudopolymeric porphyrin aggregates in aqueous solutions can be not only fibers,[8] ribbons,[9] and tubules but also sheets[6] or vesicles.[10,11] Depending upon the chemical structure of the porphyrin, different types of aggregation mechanisms can be observed from laterally to axially stacked aggregates. A great amount of work has been devoted to identify the role of $\pi-\pi$ interactions in the cofacial or lateral molecular arrangements with favorable offsets of their centers.[12] Lateral aggregation can be favored if side chains are involved in hydrogen bonds and is characterized by a strong apparent exciton splitting and shift of the Soret band.[13,14]

We present here the aggregation properties of a Zn(II) complex of a long-chain triester of *meso*-tetrakis[*p*-carboxy]-phenyl porphyrin (ZnP3) in saturated hydrocarbons. In addition to the classical extended $\pi-\pi$ interactions between the porphyrinic core, the presence of both Zn metallic element and a carboxylic ligand leads to a remarkable formation of nanorods having a specific molecular arrangement with tetrameric associations.

2. Experimental Section

2.1. Synthesis. Zn(II) porphyrinic triester complex (Scheme 1) was first obtained as a side product during purification of the corresponding tetraester on a basic alumina column.[15,16] This procedure constitutes, *in this special case*, a good method of preparation of a porphyrinic linear triester monoacid (yield 40−60%) from a tetraester as the diester diacids are not encountered

* To whom correspondence should be addressed.
† UMR 5819 CEA-CNRS-Université J. Fourier.
‡ Institut Laue Langevin.
§ UMR 5046 CEA-CNRS-Université J. Fourier.

(1) Abdallah, D. J.; Weiss, R. G. *Adv. Mater.* **2000**, *12*, 1237.
(2) Terech, P.; Weiss, R. G. *Chem. Rev.* **1997**, *97*, 3133.
(3) Gust, D.; Moore, T. A. *Science* **1989**, *244*, 35.
(4) Barkigia, K. M.; Melamed, D.; Sweet, R. M.; Smith, K. M.; Fajer, J. *Spectrochim. Acta, Part A* **1997**, *53*, 463.
(5) Hunter, C. A.; Hyde, R. K. *Angew. Chem., Int. Ed. Engl.* **1996**, *35*, 1936.
(6) Endisch, C.; Böttcher, C.; Fuhrhop, J.-H. *J. Am. Chem. Soc.* **1995**, *117*, 8273.
(7) Komatsu, T.; Yamada, K.; Tsuchida, E.; Siggel, U.; Böttcher, C.; Fuhrhop, J.-H. *Langmuir* **1996**, *12*, 6242.
(8) Fuhrhop, J.-H.; Demoulin, C.; Boettcher, C.; Köning, J.; Siggel, U. *J. Am. Chem. Soc.* **1992**, *114*, 4159.
(9) Fuhrhop, J.-H.; Bindig, U.; Siggel, U. *J. Am. Chem. Soc.* **1993**, *115*, 11036.
(10) Tsuchida, E.; Komatsu, T.; Toyano, N.; Kumamoto, S.; Nishide, H. *J. Chem. Soc., Chem. Commun.* **1993**, 1731.
(11) Tsuchida, E.; Komatsu, T.; Arai, K.; Yamada, K.; Nishide, H.; Fuhrhop, J.-H. *Langmuir* **1995**, *11*, 1877.
(12) Hunter, C. A.; Sanders, J. K. M. *J. Am. Chem. Soc.* **1990**, *112*, *14*, 5525.
(13) Kasha, M.; Rawls, H. R.; El-Bayoumi, M. *Radiat. Res.* **1963**, *20*, 55.
(14) Kasha, M.; Rawls, H. R.; El-Bayoumi, M. A. *Pure Appl. Chem.* **1965**, *11*, 371.
(15) Ramasseul, R.; Maldivi, P.; Marchon, J. C. *Liq. Cryst.* **1993**, *13*, 729.
(16) Terech, P.; Gebel, G.; Ramasseul, R. *Langmuir* **1996**, *12*, 4321.

10.1021/la034341c CCC: $25.00
Published on Web 11/15/2003

Scheme 1. Transformation of ZnP4 to ZnP3[a]

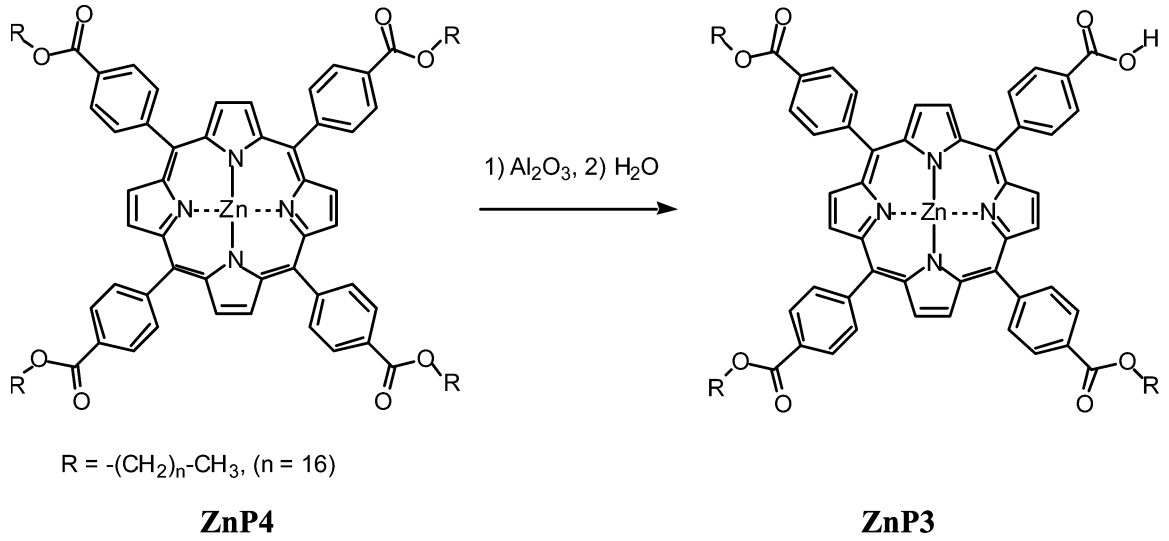

[a] The four-fold symmetry of ordinary porphyrins is lost in ZnP3.

and as the fraction of nonsaponified tetraester can be recovered and recycled.

Solvents and chemicals were used without purification unless indicated. Zinc complexes of porphyrin tetraesters were prepared according to previously published procedures[15] Analytical thin-layer chromatography was performed using Merck precoated silica plates 60F-254 (layer thickness 0.25 mm). Silica gel (230−400 mesh) was used for column chromatography. UV−visible spectra were recorded on a Perkin-Elmer Lambda 9 instrument (quartz Hellma cells with an optical path of 1 mm were used).

Preparation of Zinc(II) 5-(*p*-Carboxyphenyl)-10,15,20-tris[((*p*-hexadecyloxy)carbonyl)phenyl] Porphinate (ZnP3). A 0.3 g portion of zinc(II) 5,10,15,20-tetrakis[((*p*-hexadecyloxy)-carbonyl)phenyl] porphinate in 5 mL of CH_2Cl_2 is placed on the top of a chromatographic column prepared with 300 g of basic alumina and CH_2Cl_2 containing 0.2% of ethanol. The zinc complex is slowly eluted with CH_2Cl_2 containing 0.2% of ethanol. About half of the complex is fixed on the column which remains pink. The nonfixed complex in CH_2Cl_2 solution is recovered at the bottom of the column. The following sequence of eluants produce the transformation of the tetraester to triester on the column: CH_2Cl_2/EtOH (95:5; 500 mL), CH_2Cl_2/EtOH (80:20; 500 mL), CH_2Cl_2/EtOH (50:50; 500 mL), EtOH, EtOH/H_2O (60:40). The Zn(II) porphyrinic triester monoacid is eluted by a one-phase mixture of the solvents EtOH (ca. 25%), Et_2O (ca. 25%), CH_2Cl_2 (ca. 25%), toluene (ca. 25%), and H_2O (ca. 3%) with a 40−60% yield. To improve its purity, the complex is eluted either on a column of silica with mixtures of CH_2Cl_2 and ethanol (up to 6%) or on silica plates with the same eluant.

F = ca. 190°, UV−vis (CH_2Cl_2) λ_{max} = 425, 555, and 595 nm. ^{1}H NMR (200 MHz, $CDCl_3$): δ (ppm) 8.925 and 8.91 (β-pyrrolic protons), 8.51 and 8.34 (2 doublets J = 8.3 Hz, ortho and meta protons near CO_2H), 8.40 and 8.28 (two doublets J = 8.3 Hz, ortho and meta protons near CO_2CH_2), 4.45 (triplet J = 6.5 Hz CO_2CH_2 protons), 1.88 (multiplet $CO_2CH_2CH_2$ protons), 1.23 (multiplet CH_2 protons), 0.82 (triplet, J = 6.4 Hz, CH_3 protons).

2.2. Scattering (SANS). For scattering experiments, the ZnP3 molecule ($C_{96}H_{124}N_4O_8Zn$) was dissolved in deuterated cyclohexane (Sigma, purity 99%, d = 0.893 g cm^{-3}) by gentle heating at 40−50 °C and shaking. A homogeneous dark reddish solution was obtained which on cooling at room temperature becomes more or less gelatinous depending upon the concentration. In the same circumstances, the ZnP4 molecule (Scheme 1) only gives purely viscous solutions. Specimens, contained in quartz cuvettes (1 mm gap), were investigated using the neutron beams of the Institut Laue Langevin (ILL, Grenoble, France) and Laboratoire Leon Brillouin (LLB, Saclay, France).

Spectrometers were used at three distances at ILL (D11, D22) and two distances at LLB (PAXE) at appropriate wavelengths, λ, to cover the momentum transfer ($Q = 4\pi/\lambda \sin\theta$, θ being half the scattering angle) range of ca. 0.003−0.3 Å^{-1}. The detectors were bidimensional, and the radial averaging of isotropic two-dimensional (2D) data was done with usual corrections for background subtractions, transmission, and normalization steps.

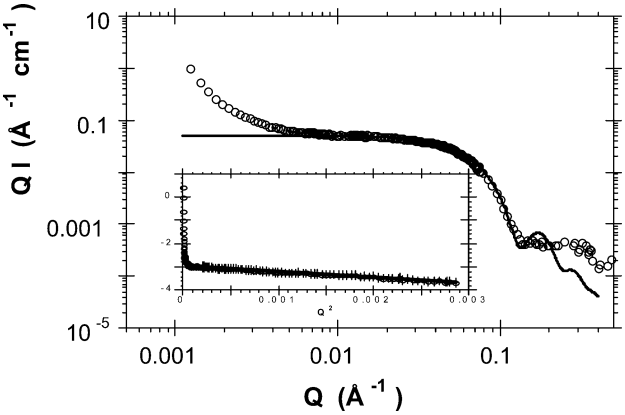

Figure 1. Typical SANS scattering curve QI vs Q (●, ILL neutron source) of a ZnP3/cyclohexane-d solution at C = 0.0041 g cm^{-3}. Full line is the theoretical scattering behavior for long rods with r_0 = 31.4 Å and a radial Gaussian polydispersity ($\epsilon = \Delta r/r_0$ = 0.12) also including the instrumental resolution contribution. Insert: Guinier plot ln(QI) vs Q^2, from the straight part a value for the cross-sectional radius of gyration r_c = 22.2 Å is extracted (see text).

3. Results and Analysis

The ZnP3/cyclohexane-d system is composed of rodlike aggregates as previously shown[16] and recalled in Figure 1 with a typical small-angle neutron scattering curve. In a QI versus Q representation, the low-Q plateau clearly points at the unidirectional character of the ZnP3 aggregates characterized by a Q^{-1} intensity decay (expressions 1 for large L/r aspect ratio of the rod and $2\pi/L < Q_{min}$).

$$F(\vec{Q},\alpha) = \frac{[2\sin(\vec{Q}L/2\cos\alpha)J_1(\vec{Q}r_0\sin\alpha)]}{(\vec{Q}L/2)\vec{Q}r_0\sin\alpha} \quad (1a)$$

$$I(Q) = (\Delta\rho)^2[\langle F^2(\vec{Q},\alpha)\rangle_\alpha + \langle F(\vec{Q},\alpha)\rangle_\alpha{}^2(S(\vec{Q}) - 1)] \quad (1b)$$

L is the length of the rod, r_0 is its geometrical radius, and α is the angle between the rod axis and the vector $\vec{Q}$ (its modulus after the averaging operation is denoted Q). For

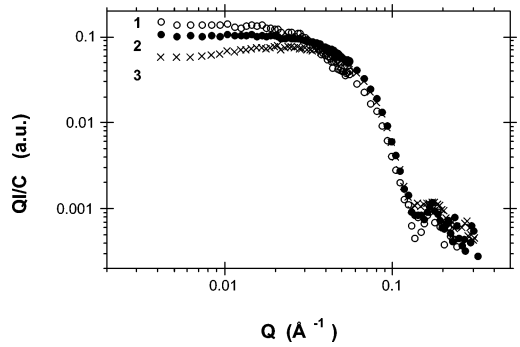

Figure 2. Variation of the cross-sectional scattering profile (QI vs Q, LLB neutron source) with ZnP3 concentration in cyclohexane-d: **1**, $C = 0.53$ wt %; **2**, $C = 1.9$ wt %; **3**, $C = 3.1$ wt %.

a dilute system, $S(Q) \sim 1$ and in absence of orientation correlations, the corresponding isotropic data are radially averaged into intensities $I(Q)$ reducing to expression 1c

$$I(Q) = \pi C M_L \Delta b^2_{spec} [2J_1(Qr)/Qr]^2 \qquad (1c)$$

with M_L being the molecular weight per unit length, $\Delta b_{spec}{}^2$ the specific neutron contrast of the aggregate, and J_1 the Bessel function of the first kind. Both the subsequent Gaussian decay and first oscillation are well reproduced by the theoretical behavior for long and rigid rods with a radius $r_0 \sim 31.4$ Å. This situation is representative of the system at a moderate concentration ($C = 0.457$ wt %). The innermost low-Q upturn is attributed to interactions between the rods and will be not further analyzed in the present study. A more detailed small-angle neutron scattering (SANS) investigation is now performed to elucidate the structure of the rods forming the fragile ZnP3 network.

First, the nature of the suspension of rodlike metalloporphyrin aggregates can be described by analyzing the scattering profiles versus ZnP3 concentration. Figure 2 shows that two scattering features are varying while two others remain unchanged. Indeed, both the low Q^{-1} decay (a plateau in the QI vs Q plot) and the Q location of the intensity oscillation ($Q = 0.17$ Å^{-1}) were unchanged. A broad bump in the intermediate Q range ($0.01 < Q < 0.035$ Å^{-1}) appears when the concentration is increased to $C \sim 3$ wt %. Simultaneously, the intensity oscillation becomes less resolved. These observations suggest that two populations of morphologies coexist as observed in the experimental Q range. Long ZnP3 rods, such that $2\pi/L < Q_{min}$ (0.004 Å^{-1}), $L > 1500$ Å, are present together with shorter rods (typically ca. 500 Å). Figure 1 is representative of moderate ZnP3 concentrations ($C < 2$ wt %) for which mainly long rods are observed. The Q^{-1} low Q decay is consistent with the large value of the $L/2r$ ratio estimated for the rodlike component while the large Q oscillation confirms that the transverse morphology remains unique when the concentration is increased. A further concentration increase modifies the scattering curve both in its intermediate Q range and in the resolution of the large Q oscillation. This phenomenology is attributed to the presence of shorter rods. It is known that micellar rods have lengths varying with concentration according to power laws involving positive exponents. Thus, it may appear contradictory to observe shorter rods when the concentration is increased. In fact, an isothermal increase of concentration induces a direct increase of the amount of unstable molecules that are in excess with respect to the solubility threshold (or critical aggregation concentration). This situation leads to an increase of the number of germination sites available for the rodlike micellar growth. In such a context, the unfavorable enthalpic excess due to the extremities of rods is counterbalanced by the entropic component due to the growing rods. This situation is preserved but the increase with concentration of growth sites, statistically makes the fraction of small rods with lengths compatible with the observation limit ($2\pi/Q_{min}$) sufficient to be now observed as a bump in a QI vs Q plot. The amplitude of the bump depends on the aspect ratio of the rods and their volume fraction. The theoretical simulation of Figure 3 shows the remarkable scattering profile for suspensions made up of long and shorter rods ($L/2r = 5$). The expected bump is well experimentally observed at $0.014 < Q < 0.04$ Å^{-1}.

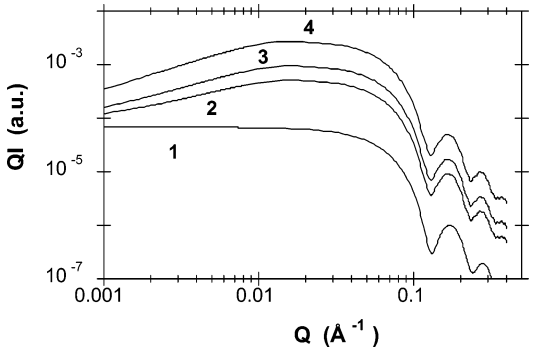

Figure 3. Theoretical form-factor scattering profile for a two-component system made up of short and long rods in a QI vs Q representation. Both long and short rods have a radius $r = 30$ Å. A Gaussian polydispersity is also included in the calculation. Different rod fractions f_R are represented. (1) $f_R = 0.0$; (2) $f_R = 0.05$; (3) $f_R = 0.1$; (4) $f_R = 0.3$.

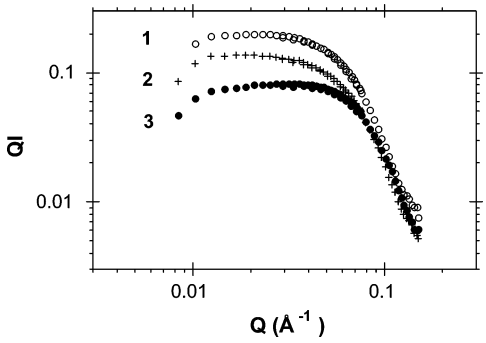

Figure 4. Variation of the cross-sectional scattering profile (QI vs Q, ILL neutron source) with the pyridine concentration at a fixed ZnP3 concentration $C = 3.5$ wt % in cyclohexane-d: **1**, (○) molar ratio r_{pyr} = [pyridine]/[ZnP3] = 0; **2**, (+) pyridine $r_{pyr} = 0.077$; **3**, (●) pyridine $r_{pyr} = 0.545$.

Such a scattering phenomenology has already been observed associated with strikingly different viscoelastic properties. With a bicopper tetracarboxylate,[17] long monomolecular and breakable threads are formed and exhibit an opposite behavior under shear. The bicopper system develops elasticity under shaking and a liquidlike behavior at rest while the ZnP3 system is liquid under shaking and gelatinous at rest!

The proportion of short rods in the network can be increased by mixing the suspension with a molecular component, named end-capper EC, whose affinity for ZnP3 is much larger than that between two ZnP3 molecules. Pyridine can play the role of an EC molecule. Figure 4 shows the influence of increasing proportions of pyridine upon the scattering profile. In parallel, it is visually evident

(17) Terech, P.; Coutin, A. *Langmuir* **1999**, *15*, 5513.

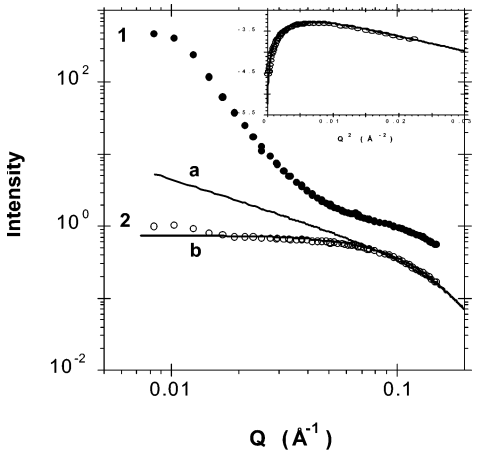

Figure 5. Comparison of the scattering profile (I vs Q, ILL neutron source) of ZnP4 in cyclohexane-d (**1**, $C = 3.1$ wt %) and in a mixture pyridine/cyclohexane-d (**2**, r_{pyr} = [pyridine]/[ZnP4] = 2.6). Full lines are theoretical curves for 22 Å diameter (d) rods: (a) long rod $L/d > 10$; (b) short disk $L/d = 2$. Insert: ln(QI) vs Q^2 plot for disks $L/d = 2$ according to expression 1a.

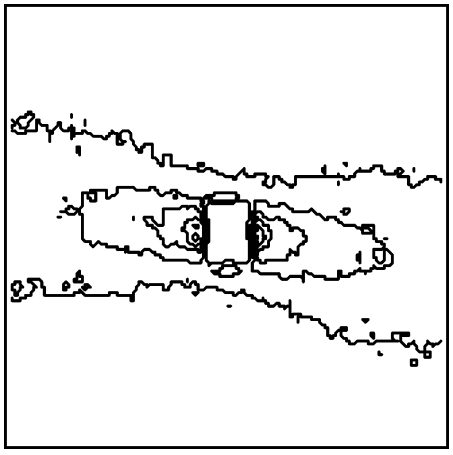

Figure 6. Isointensity neutron scattering contour plots of a ZnP3 suspension ($C = 2.5$ wt %) in cyclohexane-d at rest. The side corresponds to a 0.0−0.014 Å^{-1} Q range.

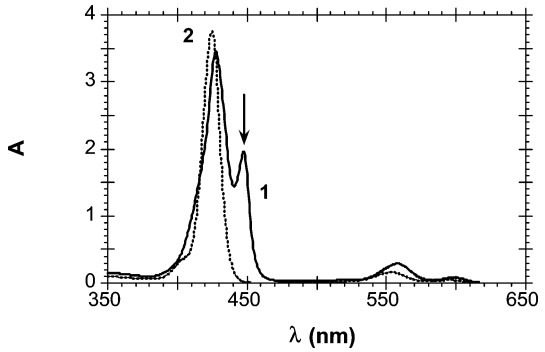

Figure 7. UV−visible absorption spectroscopy of ZnP3 dilute solutions: **1**, cyclohexane, $C = 2 \times 10^{-4}$ M; **2**, chloroform, $C = 2.2 \times 10^{-4}$ M.

that the suspensions become drastically more liquid when the pyridine proportion is raised. Two related scattering effects can be observed: (1) a decrease of the extrapolated intensity at zero Q; (2) an increase of the bump component. It is known[18] that both the average statistical contour length and the width of the polydispersity distribution function are decreased when end-capper species are competing in self-assembling reactions. At the end, rods are more or less disaggregated into pyridine-complexed ZnP3 shorter species. Small enough aggregates can be dispersed in the liquid component and no longer contribute to the low-angle scattering. Such a mechanism is consistent both with the overall decrease in scattering intensity and with the amplification of the intermediate bump (QI vs Q) while the large Q oscillation is maintained.

The particular role played by the carboxylic group can be examined by comparing the aggregation properties of ZnP3 and ZnP4 molecules (Scheme 1). It appears that ZnP4 never gives gelatinous specimens even at high concentrations (up to ca. 8 wt %). Nevertheless, concentrated solutions exhibit a scattering curve revealing the presence of large species (low-angle Q^{-4} component of curve 1 in Figure 5). Pyridine dissolves these "heterogeneities" as demonstrated in curve 2 (Figure 5) by the vanishing of the low-angle component. Curve 2 is now characteristic of finite scatterers (small disks of ca. 22 Å diameter) as characterized by the appropriate modeling of the Figure 5 insert using expressions 1a and 1b. Interestingly, the dimensions can be consistent with the aggregation of single ZnP4 molecules tilted in a small stack. It will be shown in the following that the carboxylic group in ZnP3 is responsible for a more complex aggregation mechanism. Interactions between ZnP4 species are weak enough to form only small aggregates unable to overlap.

The ZnP3 suspensions appear as highly sensitive to any orientational stimuli. The elliptical contour plot of Figure 6 shows that in a suspension ($C = 2.5$ wt %) at rest, excluded volume effects are responsible for significant orientation effects. The elliptical scattering pattern is related to the orientation distribution of rods. Rods exhibit a contribution at low angles only when they lie perpendicular to the vector $\vec{Q}$. A dilute suspension of rods shows up an isotropic scattered intensity. With oriented rods, positions and/or orientations are correlated and the scattering depends on the angular position of the system with respect to $\vec{Q}$ thus forming an anisotropic pattern. The decrease of correlation length in the perpendicular axis to the shear, and its increase along the shearing axis leads respectively to an increase of the intensity in the perpendicular direction, and to a decreasing intensity in the shear direction. An elliptical pattern with a main axis orthogonal to the orientation direction is then formed. At rest, this main axis indicates that the ZnP3 rods orient almost parallel to the long and vertical axis of the cell.

As commonly observed for rod-forming systems of the class of organogels, ZnP3 aggregation is strongly dependent upon the solvent type. In chloroform, the solubility of ZnP3 is very high and no viscoelastic effects can be observed at any concentration. UV absorption spectroscopy can be used to characterize the level of dispersion in $CHCl_3$ and the mode of molecular aggregation in cyclohexane. In chloroform (Figure 7), a single and narrow band at $\lambda = 425$ nm characterizes the molecular dispersion of ZnP3. In cyclohexane, a red shift to $\lambda = 427.8$ nm and a split to a secondary maximum at $\lambda = 447$ nm are observed. Spectral modifications at larger wavelengths will not be commented on here. Numerous calculations have been made in the past to model the charge distribution and the nature of intermolecular interactions in porphyrin systems.[12] A favorable offset or slipped geometry is often predicted and which can be evidenced by absorption spectroscopic experiments. Two types of aggregates are considered with unique electronic and spectroscopic properties. J-aggregates are formed with molecules arranged in one dimension with the angle α[19] between their transition moment and the line joining the centers of the

(18) Saville, P. M.; Sevick, E. M. *Langmuir* **1998**, *14*, 3137.

Chart 1. Aggregation Model in ZnP3 Rods[a]

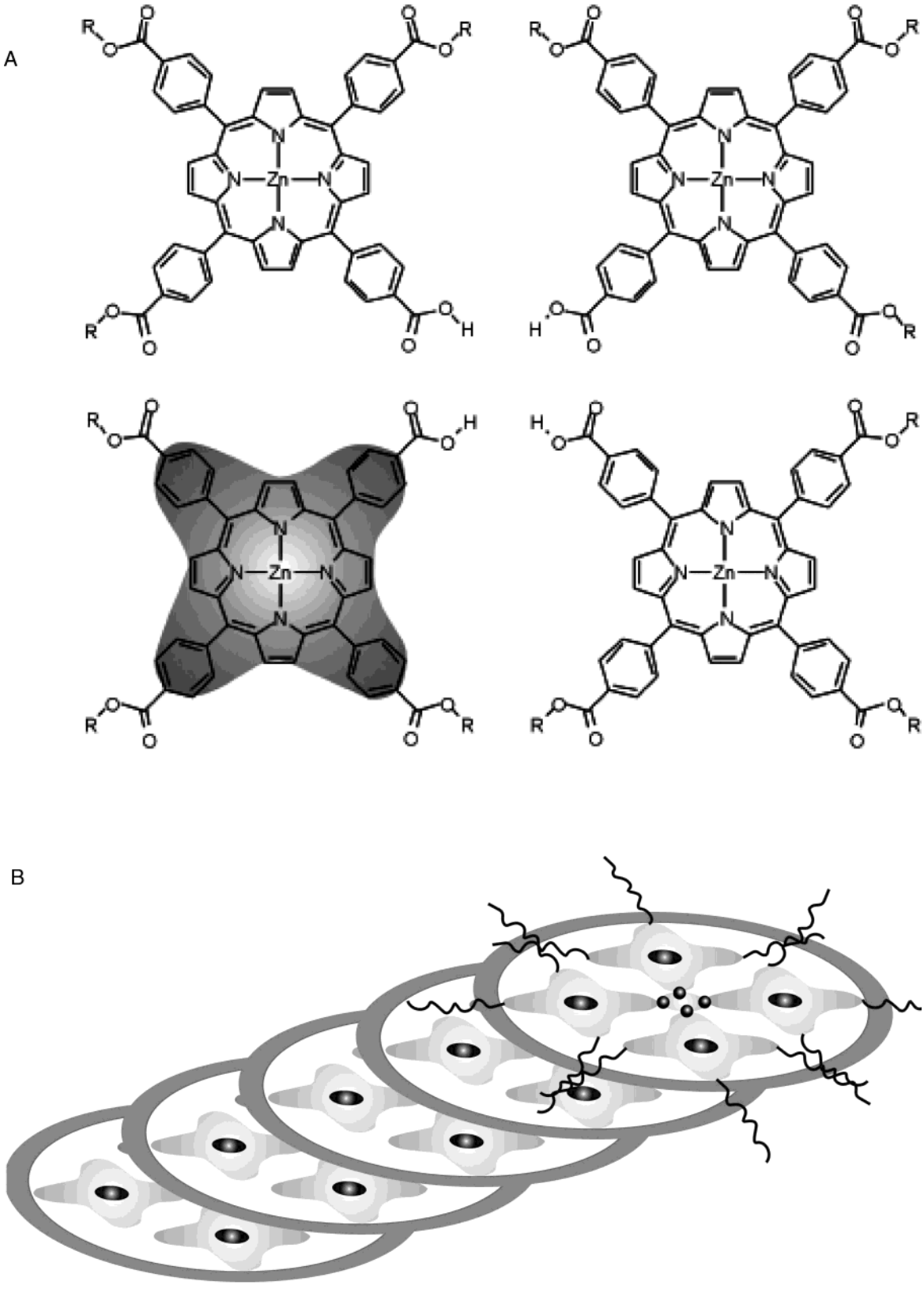

[a] (A) Tetrameric association in a rod section. The shaded area represents the porphyrinic plane. (B) Schematic representation of the ZnP3 rod. The length scale of the different atoms and parts is respected. The contrasting chemical compositions are shown from the central core, the Zn elements, the porphyrin planes, and the carbonyl shell, to the external C16 aliphatic chains.

molecules being in the range $0° < \alpha < 54.7°$. It results that the strong coupling between monomers generates a coherent excitation at red-shifted wavelengths.[20,21] On the other hand, H-aggregates are linear arrangements of molecules with the transition moments perpendicular to the axis joining the centers ($54.7° < \alpha < 90°$). The dipolar coupling leads then to a blue shift of the absorption band. In J-aggregates the molecules are arranged side-by-side while with H-aggregates they are face-to-face. In cyclohexane, the ZnP3 solution becomes translucent, scatters

light, and exhibits broadened, split, and red-shifted absorption bands associated to the formation of J-aggregates. A model (Chart 1), based on absorption spectroscopy and small-angle scattering (vide infra), is proposed and will be further discussed.

To refine the molecular description, it is useful to extract the parameter n_L (number of aggregated molecules per unit length of rod) from SANS data. The required conditions are as follows: (1) the signal does not have any low Q extra-scattering component affecting the Gaussian decay part; (2) the pure form-factor scattering is preferably isotropic. For instance, for a solution at $C = 0.0041$ g cm^{-3}, a Guinier plot provides $\ln(QI)_0 = -2.9568$ and for $\Delta\rho^2 = 29.9 \times 10^{20}$ (cm/cm^3)^2 and then n_L is found to be equal to ca. 0.76 ± 0.1 molecules Å^{-1}. An average spacing distance between two connected molecules along the rod axis can be estimated to d_{ax} ca. 5 Å. The number of molecules per cross-sectional unit of repetition along the rod axis is then $n_L\, d_{ax} \approx 4$ molecules. Thus, a model (Chart 1) of ZnP3 aggregation in cyclohexane is proposed which involves four molecules with their carboxylic groups forming a polar inner core. Characteristic distances in the ZnP3 aggregate are as follows: $d_{Zn\cdots COO}$, ca. 10 Å; diameter for the internal carboxylated hollow cavity, ca. 3−4 Å; the outer alkanic shell (C16 chains) makes a "fuzzy" surface to the cylinder (see Chart 1) with an average thickness of 8 Å. The expected global diameter d is then $2 \times 2 \times 10 + 4 + 2 \times 8 = 60$ Å. This model is also in agreement with previous X-ray scattering data[16] characterizing a radius for high electron density of ca. 15 Å corresponding to the position of the Zn elements. Consecutive layers of four ZnP3 molecules are stacked as represented in Chart 1 through $\pi-\pi$ interactions and optimized with a radial shift. The amplitude of the shift can range from ca. 4.2 Å $\sim d_{Zn\cdots N}$ to ca. 9−10 Å $\sim d_{Zn\cdots COO}$ so as to place an electron donor site facing the Zn electron acceptor site. The stepwise stacking of four ZnP3 monomeric macrocycles finally forms inclined columns.

4. Discussion

The formation of large micellar fibers is an identified phenomenon in various aqueous solutions of porphyrins.[7−10,22,23] With organic solutions, few examples are known of self-assembled porphyrin fibers[24,25] and those involving the Zn element are less frequent.[26−28] Besides synthetical metalloporphyrins, naturally occurring porphyrins can also form rodlike morphologies. For instance, chlorophylls are magnesium porphyrins playing an important role in the photosystem of green plants. It is known that aggregation develops when water is added to dry solutions of chlorophylls in nonpolar organic solvents.[29] Thus, hollow cylinders have been characterized by SANS.[24,25] Worcester et al. have shown that the diameter of the cylinders can be either 10 nm for bacteriochlorophyll *c* while bacteriochlorophyll *a* can be prepared in the form of 20 or 40 nm cylinders. With bacteriochlorophylls, aggregation involves the axial ligation between Mg(II) and the hydroxyl group of neighboring molecules strengthened by additional bonding of the hydroxyl to the keto group of ring V. Different aggregation mechanisms can be found and, for instance, with a Zn analogue[4] the molecules stack in antiparallel cofacial pairs, themselves held together by H-bonds between hydroxyl and keto groups.

A qualitative comparison of the behaviors of ZnP3 analogues (ZnP4, H2P3, H2P4, not detailed here) shows that in ZnP3 rods, the Zn element as well as the carboxylic group are determinant to establish the intermolecular connections (intra and/or inter) responsible for the formation of gelatinous specimens. ZnP3 molecules are involved in a J-aggregate with four molecules per section of rod. The complex structure of the rod is interestingly original with a shell of aliphatic chains (R), a planar π-rich layer in which is inserted a metallic (Zn) ring, and finally a polar central core (COOH) in a tilted repetition fashion. In model of Chart 1, Zn has a 5-fold coordination symmetry that allows the formation a stepwise oligomer. To compare, the structure of charged dimers of a Zn[tetra(4-carboxyphenyl)porphyrin] in water[30] has been determined by analysis of the ^{1}H NMR ring current shifts. In this case, dimers are formed in a cofacial conformation with a 3.1 Å plane-to-plane separation (simple porphyrins with no special ligands exhibit a 3.4−3.6 Å interplanar separation[12]) and an in-plane translation of 4.2 Å along the aryl−aryl axis. Such a short plane-to-plane distance is induced by the Coulombic attraction energy between the negatively and positively charged groups of these ionized porphyrins. With ZnP3, the situation is different since (i) no complementary ionic interactions exist, (ii) the solvent is apolar, (iii) ZnP3 does not have four identical substitutions, and (iiii) finally ZnP3 has a polar carboxylic group. The related red shift in the broadened Soret band absorption by exciton interaction characterizes a J-aggregate (conversely to a purely cofacial arrangement) in which the plane-to-plane distance is more likely closer to 5 Å than to 3 Å as proposed in Chart 1. In some ion-paired porphyrins, a large spacing (ca. 6.5 Å) has already been observed as a consequence of a small degree of electronic coupling.[31] A porphyrin−porphyrin distance of 7.3 Å has even been evoked in a tetrapyridyl porphyrin.[6] The variety of molecular arrangements provided by the class of porphyrins[32,33] is such that an example of a zinc(II) porphyrin complex is known in which tetramer repeating units are involved in J-aggregates.[34] A somewhat similar tetrameric association by hydrogen bonding has also been reported[35] for monopyrazolylporphyrins in chloroform solutions. The interaction between the metal (electron acceptor) and an electron donor ligand of a neighboring molecule in slipped cofacial

(19) The absorption shift $\Delta\nu$ can be written $\nu_A - \nu_M = (N-1)2\langle M^2\rangle(1 - 3\cos^2\alpha)/(4\pi\epsilon_0 N h r^3)$, where ν_A is the absorption frequency of the aggregate, ν_M is that of the monomer, M is the amplitude of the transition dipole moment, and r is the distance between the centers.

(20) Rosengarten, B.; Böttcher, C.; Schulz, A.; Fuhrhop, J.-H.; Siggel, U. *J. Porphyrins Phthalocyanines* **1998**, *2*, 273.
(21) Kobuke, Y.; Miyaji, H. *Bull. Chem. Soc. Jpn.* **1996**, *69*, 3563.
(22) Fuhrhop, J.-H.; Bindig, U.; Siggel, U. *J. Chem. Soc., Chem. Commun.* **1994**, 1583.
(23) Komatsu, T.; Nakao, K.; Nishide, H.; Tsuchida, E. *J. Chem. Soc., Chem. Commun.* **1993**, 728.
(24) Worcester, D. L.; Michalski, T. J.; Katz, J. J. *Proc. Natl. Acad. Sci. U.S.A.* **1986**, *83*, 3791.
(25) Worcester, D. L.; Katz, J. J. In *Neutrons in Biology*; Knott, S. a., Ed.; Plenum Press: New York, 1996.
(26) Jesorka, A.; Balaban, T. S.; Holzwarth, A. R.; Schaffne, K. *Angew. Chem., Int. Ed. Engl.* **1996**, *35*, 2861.
(27) Tamiaki, H.; Kubota, T.; Tanikaga, R. *Chem. Lett.* **1996**, 639.
(28) Smith, K. M.; Kehres, L. A.; Fajer, J. *J. Am. Chem. Soc.* **1983**, *105*, 1387.
(29) Katz, J. J.; Bowman, M. K.; Michalski, T. J.; Worcester, D. L. In *Chlorophylls*; Scheer, H., Ed.; CRC Press: Boca Raton, FL, 1991.
(30) Hofstra, U.; Koehorst, R. B. M.; Schaafsma, T. J. *Magn. Reson. Chem.* **1987**, *25*, 1069.
(31) Araki, K.; Wagner, M. J.; Wrighton, M. S. *Langmuir* **1996**, *12*, 5393.
(32) Fuhrhop, J.-H.; Rosengarten, B. *Synlett* **1997**, 1015.
(33) Siggel, U.; Bindig, U.; Endisch, C.; Komatsu, T.; Tsuchida, E.; Voigt, J.; Fuhrhop, J.-H. *Ber. Bunsen-Ges. Phys. Chem.* **1996**, *100*, 2070.
(34) Komatsu, T.; Yanagimoto, T.; Furubayashi, Y.; Wu, J.; Tsuchida, E. *Langmuir* **1999**, *15*, 4427.
(35) Ikeda, C.; Nagahara, N.; Motegi, E.; Yoshioka, N.; Inoue, H. *J. Chem. Soc., Chem. Commun.* **1999**, 1759.

arrangements is also encountered in other porphyrin supramolecular aggregates.[36]

Further FT-IR, UV absorption spectroscopy, and NMR studies will analyze[37] the molecular aggregation mechanism and in particular the potential implication of Zn with a carboxylic group. The rheological behavior of the rod suspensions will be the subject of a forthcoming publication.

(36) Miyaji, H.; Kobuke, Y.; Kondo, J. *Chem. Lett.* **1996**, 497.
(37) Aldebert, P.; Marechal, Y. To be submitted.

Acknowledgment. The Institut Laue Langevin (Grenoble, France) and the Laboratoire Leon Brillouin (Saclay, France) are thanked for providing access to the neutron beams and for all technical support during the experiments. The authors are grateful to C. Balbine and C. Dumon for their contribution to the synthesis work. Drs. P. Aldebert and Y. Marechal are acknowledged for interesting discussions. J. J. Allegraud is thanked for his valuable help during the modeling step of the work.

LA034341C